Ultrathin Silica Membranes with Highly Ordered and Perpendicular Nanochannels for Precise and Fast Molecular Separation

Journal:	*ACS Nano*
Manuscript ID:	nn-2015-048873
Manuscript Type:	Article
Date Submitted by the Author:	06-Aug-2015
Complete List of Authors:	Lin, Xingyu; Zhejiang University, Chemistry Yang, Qian; Zhejiang University, Chemistry Ding, Longhua; Zhejiang University, Chemistry Su, Bin; Zhejiang University, Chemistry

TOC

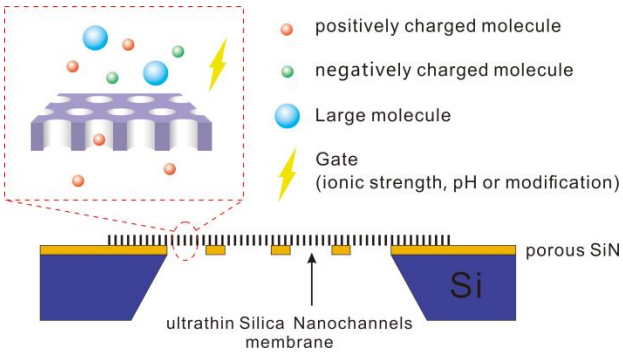
positively charged molecule
negatively charged molecule
Large molecule
Gate
(ionic strength, pH or modification)
porous SiN
Si
ultrathin Silica Nanochannels membrane

Ultrathin Silica Membranes with Highly Ordered and Perpendicular Nanochannels for Precise and Fast Molecular Separation

*Xingyu Lin, Qian Yang, Longhua Ding, Bin Su**

Institute of Microanalytical Systems, Department of Chemistry & Centre for Chemistry of High-Performance and Novel Materials, Zhejiang University, Hangzhou 310058, P. R. China

* E-mail: subin@zju.edu.cn

KEYWORDS: Ultrathin Membrane; Nanochannel; Silica; Ion Transport; Molecular Separation

ABSTRACT: Membranes with the ability of molecular/ionic separation offer potential in many processes ranging from molecular purification/sensing, to nanofluidics and to mimicking biological membranes. In this work we report the preparation of a perforative free-standing ultrathin silica membrane consisting of straight and parallel nanochannels with a uniform size (~ 2.3 nm) for precise and fast molecular separation. Due to its small and uniform channel size, the membrane exhibits a precise selectivity towards molecules based on size and charge, which can be tuned by ionic strength, pH or surface modification. Furthermore, the ultrasmall thickness (10 – 120 nm), vertically aligned channels and high porosity (4.0 – 10^{12} pores cm^{-2}) give rise to a significantly high molecular transport rate. In addition, the membrane also displays excellent stability and can be consecutively reused for a

month after washing or calcination. More importantly, the membrane fabrication is convenient, inexpensive and does not rely on sophisticated facilities or conditions, providing potential applications in both separation science and micro/nanofluidic chip technologies.

Artificial membranes with the ability of molecular separation have received considerable attentions, considering their potential applications in sample purification,[1-3] water desalination,[4] nanofluidics,[5, 6] molecular sensing,[7] drug delivery,[8, 9] nanoconfinement study[10, 11] and mimicking biological membranes.[12, 13] Conventional membranes based on the nonsolvent-induced phase separation are not suitable for molecule separation because of their broad pore size distributions.[14, 15] For this purpose, membranes consisting of ultrasmall and uniform nanopores/nanochannels of molecular dimension are highly desired,[16] where steric forces, electrostatic interactions and van der Waals forces play important roles. Usually, a sub-10 nm nanochannel is needed to precisely separate molecules, such as small ions, organic molecules, DNA, proteins and so on.[1, 2, 17-24] Furthermore, the membranes should be ultrathin and highly porous in order to achieve a high molecular transport rate and flux.[14, 16] In addition, the membranes should also have adequate chemical/thermal/mechanical stability for operation under different conditions, should be ease of fabrication and can be mass-produced at a low cost.

Various isoporous nanofabricated membranes have been so far fabricated,[25] such as nanolithographic membranes,[26] anodic aluminum oxide (AAO) membranes,[1, 27, 28] track-etched membranes,[24, 29-31] block copolymers (BCP) self-assembled membranes,[32-34] carbon nanotubes (CNTs) membranes[21, 22, 35, 36] and graphene/graphene oxide membranes,[4, 19,

[20, 37] and so on. Nanolithography technologies, such as electron beam lithography and focused electron/ion beam, can be used to fabricate nanopores on various substrates,[26] yet they are expensive and usually unable to fabricate a high density of pores smaller than 10 nm precisely. AAO and track-etched membranes are commercially available but usually consist of channels larger than 10 nm,[25] and precise post-modification is required to reduce the channel size for molecular separation.[1, 24, 27, 28, 30, 31] The micrometer-scale thickness of AAO and track-etched membranes also limits significantly the molecular transport rate.[16] BCP self-assembled membranes have been prepared for biomolecular separation,[32-34] however their thermal, chemical and mechanical stability need to be improved.[25] Membranes consisting of vertically aligned CNTs with 7 nm[21] or sub-2 nm[22, 38] channels have also been fabricated for molecular separation,[13, 21, 39, 40] as well as biomimetic cell membrane,[13] electrophoresis[38] and electroosmotic flow studies.[41] However, parallel and vertical alignment of CNTs needs relatively harsh conditions and involves complex processing, and the membranes are relatively thick. Recently, graphene/graphene oxide membranes have been intensively studied for molecular sieving and water desalination,[4, 19, 20, 37] yet their stability in water[42] and low molecular flux due to the limited porosity[37] are challenged. Moreover, nanolithography techniques are still needed to produce pores in the single-layer graphene, thereby the pore size or density cannot be well controlled.[4, 20, 43] Until now, fabrication of ultrathin membranes with a high density of uniform ultrasmall nanochannels/nanopores remains challenging.

Mesoporous silica films consisting of well-ordered and vertically aligned nanochannels on solid substrates have been prepared using different methods.[44-47] These films are ultrathin

and highly porous. Furthermore, the size of nanochannels is uniform and can be tuned from 1.6 nm to 8 nm by properly controlling the synthetic conditions.[47-49] In addition, they can be mass-produced at a low cost. These characteristics make them excellent candidates for molecular separation. Herein, we report a facile approach to prepare free-standing silica nanochannel membranes (SNMs) with perforative channels and its integration with a microfluidic device for precise and fast molecular separation. The fabrication is convenient, inexpensive and can be accomplished in an ordinary chemistry lab, relying on neither expensive facilities nor harsh conditions. Due to the small and narrow size distribution of silica nanochannels (~ 2.3 nm, negatively charged), SNMs exhibit a precise selectivity towards molecules based on size and charge, which can be tuned by ionic strength, pH or surface modification. The molecular flux across the SNMs is considerably high in comparison with commercial membranes with even larger pores, due to their ultrasmall thickness (10 – 120 nm), perpendicular and parallel channels, and high porosity (16.7%, 4.0×10^{12} pores cm^{-2}). In addition, the SNMs have excellent chemical, thermal and mechanical stability and can be repeatedly used.

RESULTS AND DISCUSSION

Preparation of Perforated SNMs. SNMs were primarily prepared on the indium tin oxide (ITO) glass by the Stöber-solution growth approach.[46] The growth time was set to 12 h unless otherwise specified. The SNM on the ITO, designated as SNM/ITO, was proved to be crack-free by cyclic voltammetry measurements before and after removal of surfactant templates (see **Figure S1**). A poly(methyl methacrylate) (PMMA)-assisted approach (as

illustrated in **Figure 1a-f**) was used to transfer the SNM from ITO glass to various porous substrates with much larger pores, such as porous silicon nitride (p-SiN) chip, track-etched polyethylene terephthalate (PET) film, capillary plate and perforated silicon wafer (see Methods). Briefly, a thin layer of PMMA was firstly spin-coated on the top of SNM/ITO. Subsequently, the PMMA/SNM/ITO was immersed in 2 M HCl solution to etch ITO, resulting in the exfoliation of PMMA/SNM from the glass surface (To be noted that the direct chemical etching without PMMA supporting led to the fragmentation of SNM, making the following operation extremely hard). Then, a porous substrate was used to fish the PMMA/SNM, followed by dissolving the top PMMA layer in acetone.

Figure 1g, **h** shows the photograph and cross-section structure of SNM/p-SiN chip, respectively. The p-SiN chip consists of a 150-nm-thick p-SiN layer supported by a 10 mm × 10 mm silicon wafer, in the center of which there is a window of 1 mm × 1 mm. It appears as a bright square and is designated as p-SiN window in the context. As shown in **Figure 1g**, the successfully transferred SNM apparently covers the whole p-SiN window. On the p-SiN window, there is an array of 4-μm-diameter SiN pores with a pore-to-pore distance of 30 μm, as seen in the scanning electron microscopy (SEM) image (**Figure 2a**). After the SNM was transferred, the micrometer pores were fully covered with an ultrathin and smooth layer of SNM without any visible cracks (**Figure 2b**). Given the thickness of SNM is only ca. 60 nm, micrometer pores on the p-SiN window can be still resolved by SEM. To be mentioned that the SiN pores were fabricated by photolithography and dry/wet etching, thus there are a large number of tiny tracks and pits on the SiN surface (**Figure S2**). After being covered with the SNM, the p-SiN surface turned very smooth, indicating the successful transfer of SNM. The

photographs and SEM pictures of SNMs transferred to other porous substrates, such as track-etched PET film (containing 2 μm channels), capillary plate (containing 10 μm channels) and perforated silicon wafer (containing a 25 μm pore), are displayed in **Figure S3**. With the support of these porous substrates, the resulting SNM can be easily handled and used.

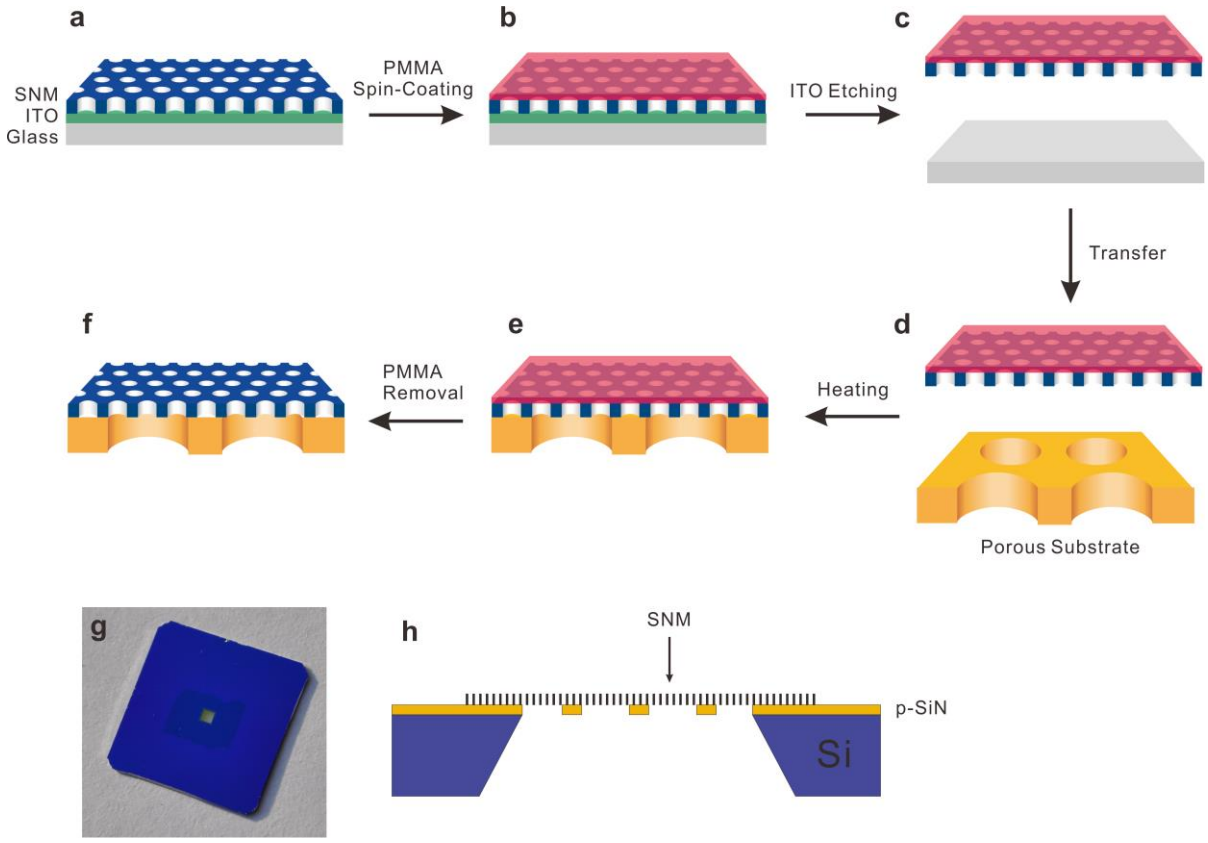

Figure 1. (a-f) Illustration of PMMA-assisted transfer method for the fabrication of perforated SNM: (a) SNM grown on the ITO glass. (b) Spin coating of PMMA on the top of SNM. (c) Etching ITO layer in 2 M HCl to segregate the SNM and glass. (d) Fishing the segregated SNM with another porous membrane. (e) Heating treatment to reinforce the bonding between SNM and the porous substrate. (f) Removal of PMMA by dissolving in acetone. (g) Photograph of SNM transferred to the p-SiN chip that consists of an array of micrometer-sized holes. The SNM appears as the rectangle with irregular edges. (h) Schematic illustration of the cross-section structure of SNM/p-SiN chip.

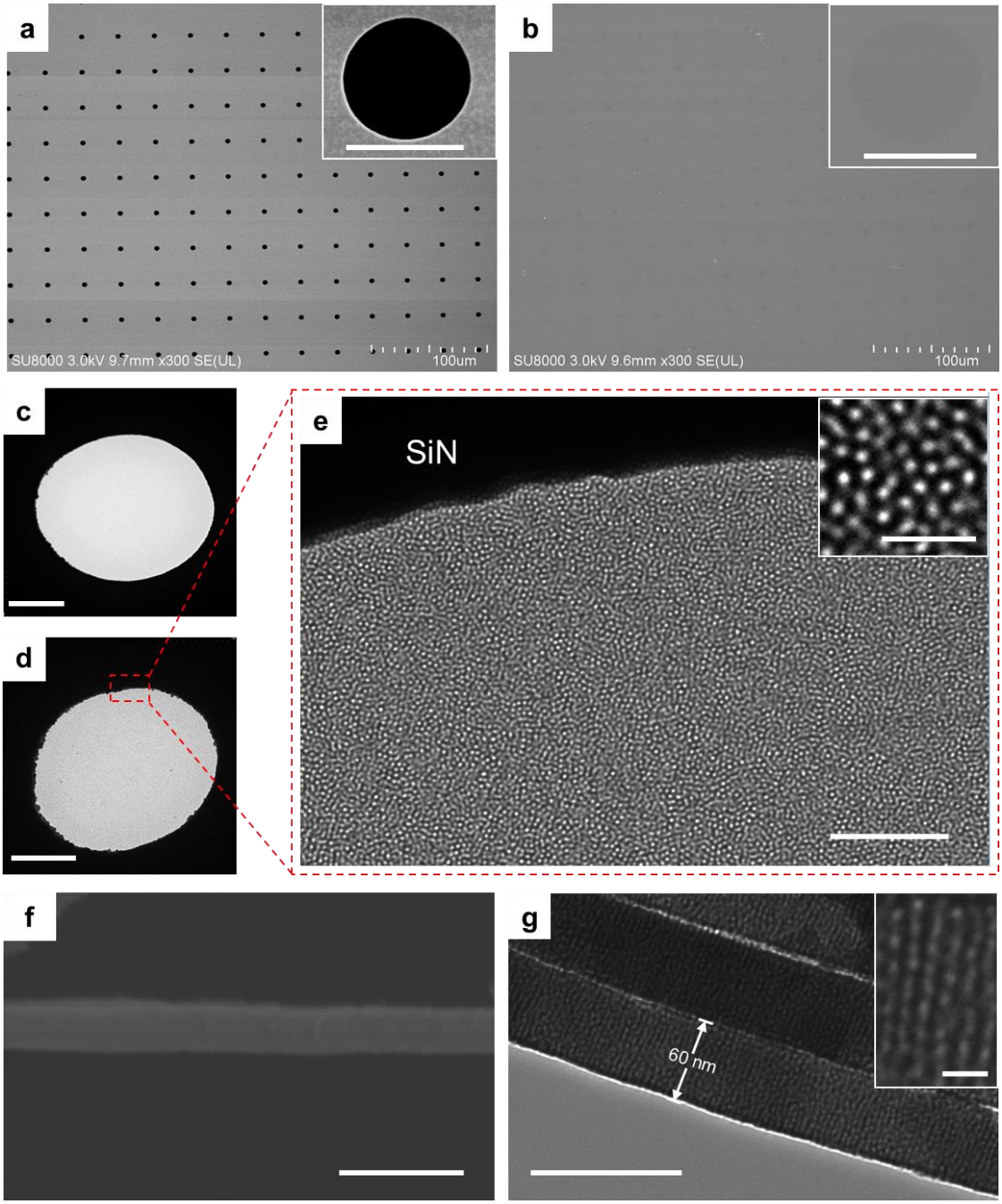

Figure 2. (a, b) Top-view SEM images of a bare p-SiN (a) and SNM/p-SiN (b). The insets show a single microhole before (a) and after (b) supporting SNM. The scale bar is 4 μm. (c, d) Top-view TEM images of a single microhole before (c) and after (d) supporting SNM. The scale bar is 1 μm. (e) High-magnification top-view TEM image of the free-standing SNM. The scale bar is 100 nm. The inset shows the magnified image with the scale bar of 20 nm. (f, g) Cross-section SEM (f) and TEM (g) images of SNM. The scale bars are 200 μm and 100 nm, respectively. The inset in (g) shows the magnified image with the scale bar of 10 nm.

The surface morphology and pore structure of ultrathin SNM supported on the p-SiN chip were characterized by transmission electron microscopy (TEM). The specimen was prepared by transferring the SNM to a 3-mm-diameter p-SiN chip, which can be positioned directly onto the TEM sample holder for observation. **Figure 2c**, **d** compare the TEM images of a single p-SiN pore before and after SNM transfer, showing clearly that the ultrathin SNM indeed covers the micrometer pore without defects/cracks (see more TEM images in **Figure S4**). From the high-magnification TEM image (**Figure 2e**), the free-standing SNM possesses an uniform pore size (~ 2.3 nm)[46] and a high porosity (16.7%, 4.0×10^{12} pores cm^{-2}). In comparison with the TEM image of SNM mechanically scraped from the ITO electrode, the PMMA-assisted transfer did not vary the surface morphology or pore structure of SNM (**Figure S4**). In addition, the cross-section SEM (**Figure 2f**) and TEM (**Figure 2g**) images show that the SNM grown for 12 h has a thickness of ca. 60 nm and consists of vertically aligned nanochannels parallel to each other with a uniform channel size.

To be noted that the thickness of SNM grown on the ITO glass surface can be easily controlled by the adjustment of the growth time, for examples, 4 h for 14 ± 2 nm, 5 h for 18 ± 4 nm, 6 h for 29 ± 4 nm, 12 h for 60 ± 3 nm and 24 h for 118 ± 6 nm. All these SNMs can be successfully transferred to the p-SiN chip (**Figure S5**). In addition, SNMs grown by the electrochemically assisted self-assembly (EASA) method[45] (**Figure S6**) can be also transferred using this approach.

On the other hand, the SNM and p-SiN chip can chemically bond together strongly, given both are rich of silanol groups on the surface.[29] Thus the supported SNM possesses

excellent thermal and chemical stability. It remained stable even after calcination at 550 °C for 6 h or immersion in a hot piranha solution for 4 h (**Figure S7**).

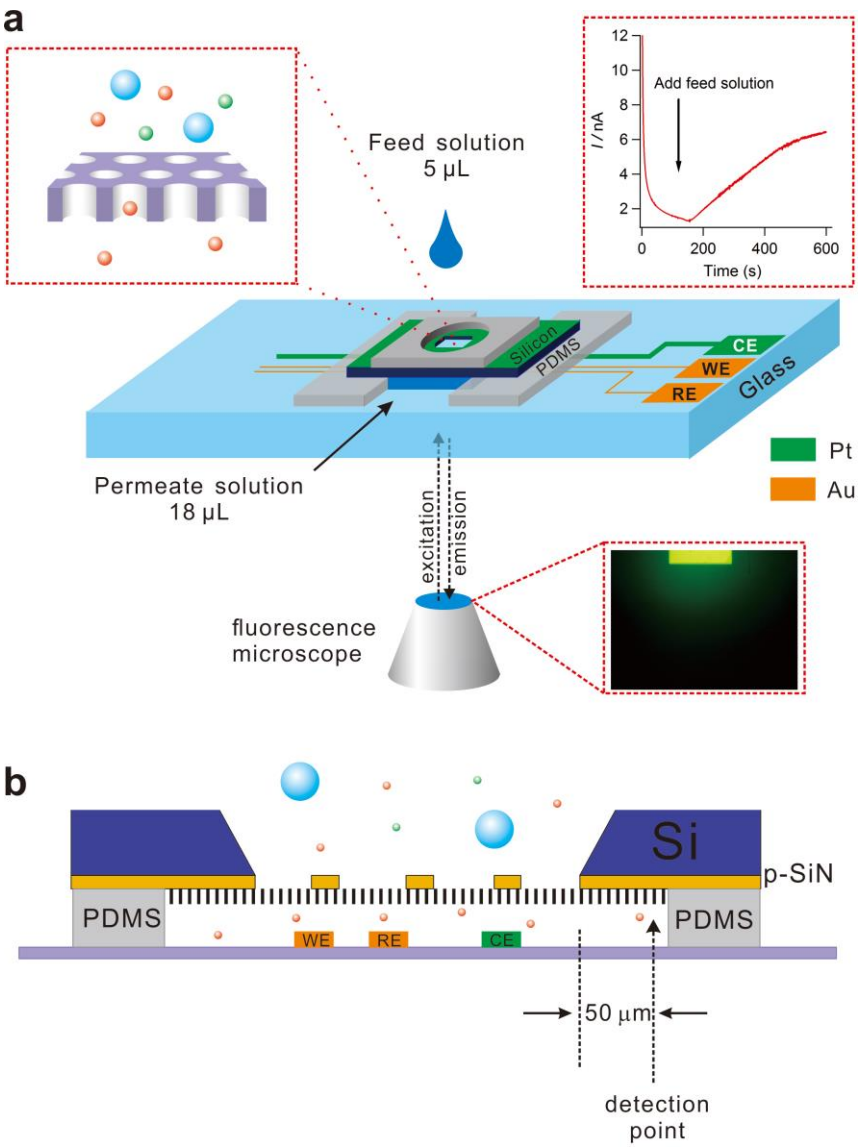

Figure 3. Schematic illustration of the permeation experiments conducted on a microfluidic chip: 3D view (a) and cross-section view (b).

Size-Based Molecular Separation. The molecular transport across the ultrathin SNM was investigated using a microfluidic device coupled with fluorescence or electrochemical detection (see Methods and **Figure 3**).[2] The SNM/p-SiN chip was positioned on a glass

slide with two 380-μm-thick polydimethylsiloxane (PDMS) gaskets, forming a micro-chamber beneath the membrane to hold the blank buffer, designated as the permeate solution. Another PDMS film with a 3 mm circular well was put on the top of the SNM/p-SiN chip to carry the feed solution containing a fluorescent/electrochemical probe. In the fluorescence detection, an inverted fluorescence microscope was used to real-time record the permeation process. The fluorescence intensity at the point of 50 μm far away from the p-SiN window edge was analyzed and plotted against the time. In the electrochemical detection, three electrodes were fabricated on the glass slide and current–time curves were recorded at constant applied potentials. Compared with the conventional U-tube setup,[24] this microfluidic device has several advantages, such as less reagent consumption, short separation time and real-time detection.

To evaluate the performance of ultrathin SNM for molecular sieving by size, we chose three cationic fluorophores, $Ru(bpy)_3^{2+}$ (bpy = 2,2'-bipyridine), $Ru(phen)_3^{2+}$ (phen = 1,10-phenanthroline) and $Ru(dpp)_3^{2+}$ (dpp = 4,7-diphenyl-1,10-phenanthroline), which possess the same charge, counterion and similar structure but different size (see structures in **Figure S8a**). In both the feed and permeate solutions, 1 mM phosphate buffer (PB, pH = 6.5) was dissolved. **Figure 4a**, **b** show the fluorescence images and kinetic plots of permeation of individual fluorophores (Time-lapse movies can be found in Supplementary **Videos S1–3**). The permeation of $Ru(bpy)_3^{2+}$ (diameter (d) = 1.3 nm) and $Ru(phen)_3^{2+}$ (d = 1.3 nm) through the SNM were observed as the appearing and gradually spreading of fluorescence signal around the membrane edge (**Figure 4a**, right). Moreover, they permeate through the SNM at almost similar rate, because they have the similar size and are smaller than that of

nanochannels in SNM. In contrast, no permeation was observed for $Ru(dpp)_3^{2+}$ (d = 2.0 nm) within several minutes, indicating its permeation was blocked or slowed down significantly, considering its size approaches to that of nanochannels according to the hindered theory.[50]

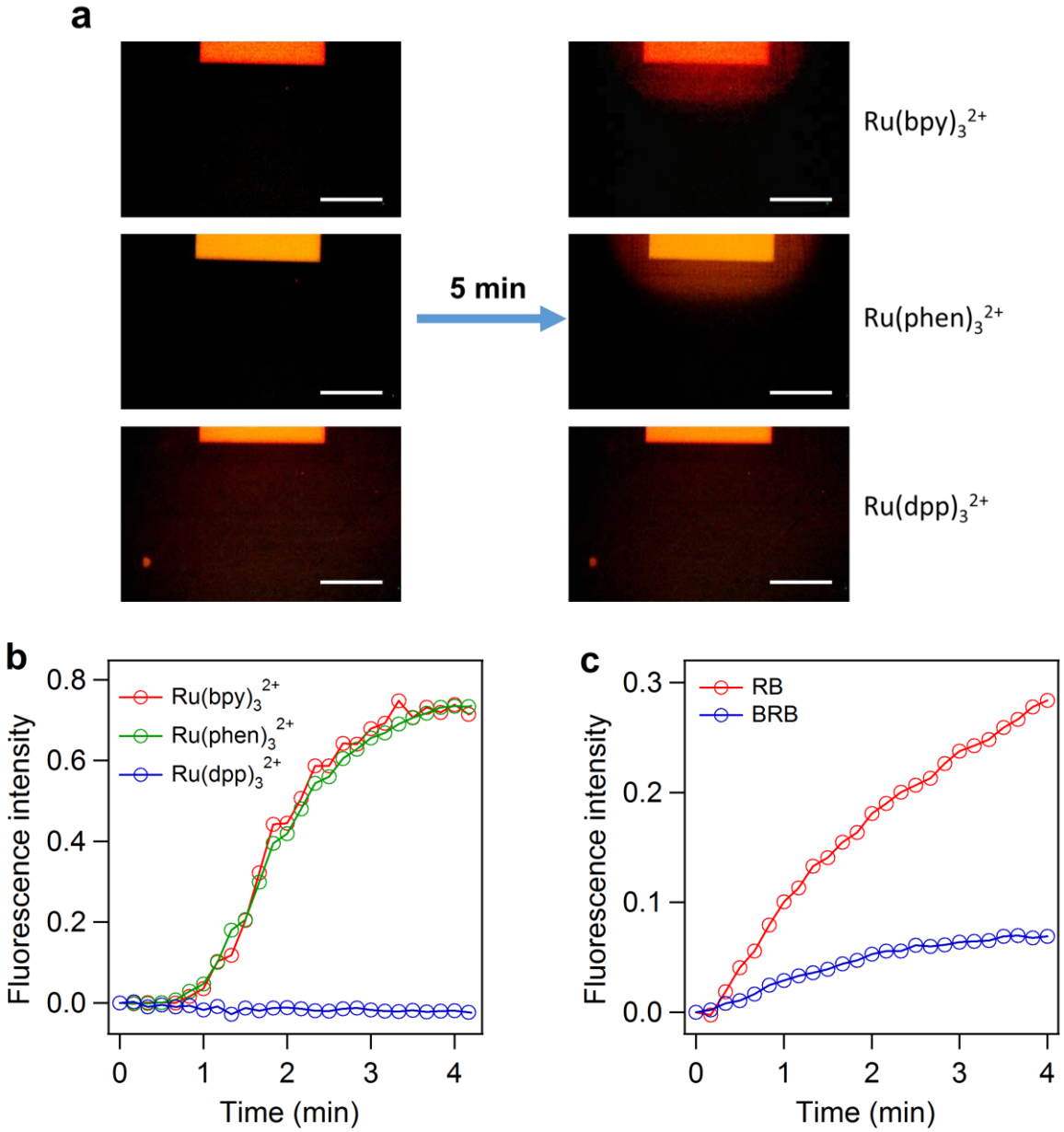

Figure 4. (a) Fluorescence images of permeation of 60 μM $Ru(bpy)_3^{2+}$, $Ru(phen)_3^{2+}$ and $Ru(dpp)_3^{2+}$ captured at 0 min (left) and 5 min (right). In order to see clearly by naked eyes, the brightness of all these images was enhanced. The scale bar is 500 μm. (b) Permeation kinetic plots of $Ru(bpy)_3^{2+}$, $Ru(phen)_3^{2+}$ and $Ru(dpp)_3^{2+}$ through SNM. (c) Permeation kinetic plots of RB and BRB through SNM.

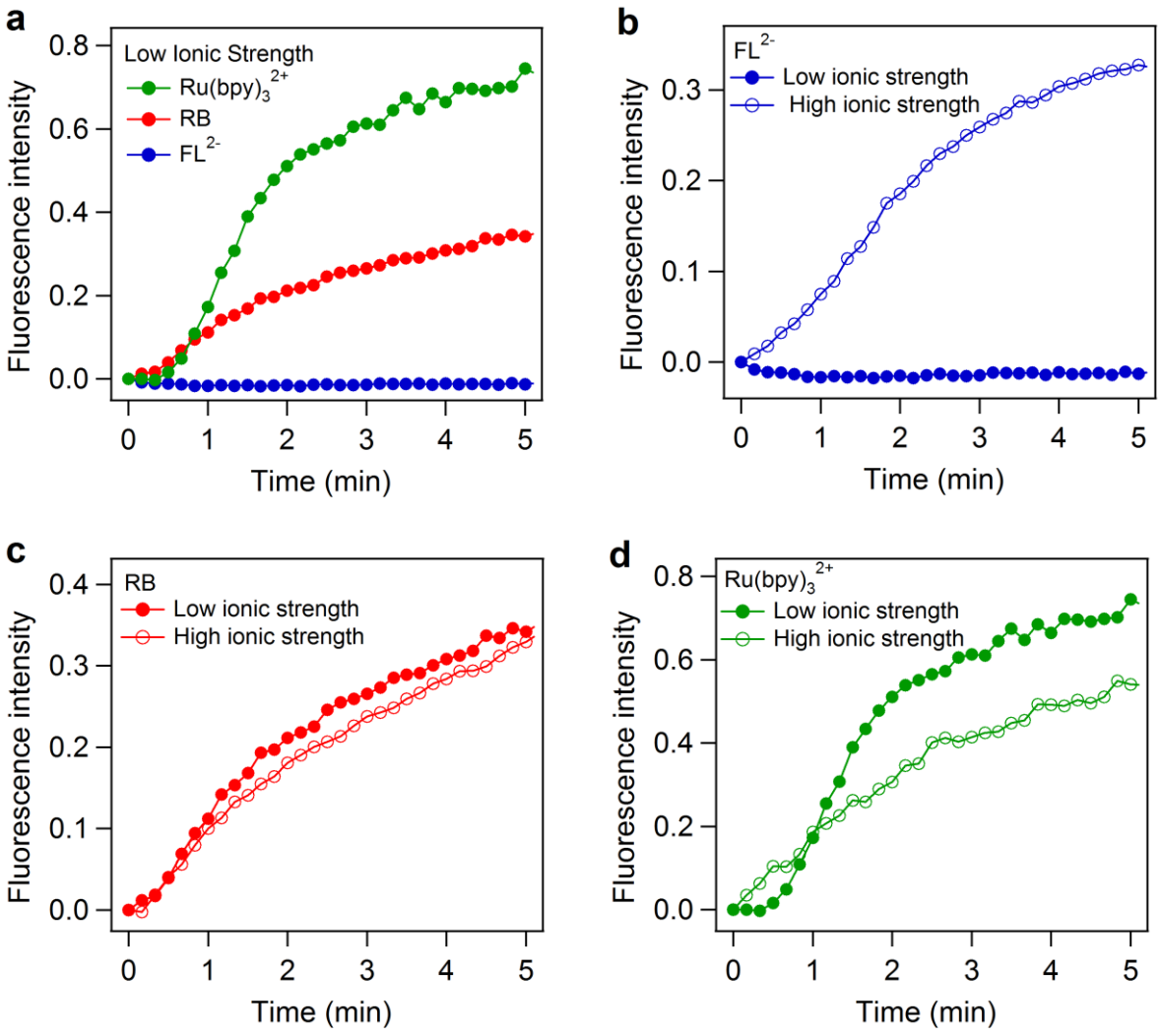

Figure 5. (a) Permeation kinetic plots of FL^{2-}, RB and $Ru(bpy)_3^{2+}$ through SNM at a low ionic strength. (b, c, d) Permeation kinetic plots of FL^{2-} (b), RB (c) and $Ru(bpy)_3^{2+}$ (d) at the low and high ionic strength.

We also studied another pair of molecules, rhodamine B (RB, d = 1.5 nm) and butyl rhodamine b (BRB, d = 1.7 nm) (see structures in **Figure S8b**). As shown in **Figure 4c**, the permeation of RB is about four times more rapid than that of BRB, although BRB is only slightly larger than RB by about 0.2 nm due to the butyl group. It suggests that the SNM can separate molecules precisely in terms of their size. To be mentioned here that both feed and permeate solutions contained a very high concentration of electrolytes, namely 1 M KCl and

1 mM PB (pH = 6.5). A high concentration of electrolytes can eliminate the impact of electrostatic interaction and thus the result reflects only the size selective nature of SNM.

Charge-Based Molecular Separation. Electrostatic interaction plays an important role in molecular separation, particularly in charged nanochannels of a few nanometers. The SNM surface and nanochannel walls are covered with a layer of silanol groups, and thus became negatively charged due to the deprotonation of silanol groups at pH higher than its pK_a. As a consequence, the nanochannels display charge permselectivity. Namely, only positively charged and neutral molecules will be expected to permeate through the SNM, whereas the negatively charged ones will be excluded from the nanochannels by electrostatic forces. We tested the SNM selectivity based on the molecular charge by performing permeation experiments with three fluorophores: fluorescein anion (abbreviated as FL^{2-}), RB and $Ru(bpy)_3^{2+}$. These three molecules have the similar size but carry different charges (see structures in **Figure S8c**). **Figure 5a** shows the quantitative permeation results of three fluorophores with the feed and permeate solutions containing only 1 mM PB (pH = 6.5) (Time-lapse movies can be found in Supplementary **Videos S4–6**). Apparently, no fluorescence was detected in the permeate solution for FL^{2-}, confirming that the SNM indeed does not allow the negatively charged molecules to pass through. In contrast, the permeation of $Ru(bpy)_3^{2+}$ is very fast due to the electrostatic attraction force. While the neutral RB is free of electrostatic interaction with the membrane and channel walls, thus its permeation is slower than $Ru(bpy)_3^{2+}$ but faster than FL^{2-}.

In principle, the charge permselectivity of silica nanochannels arises from the overlap of electric double layer (EDL) at the channel wall surface. According to the Debye-Hückel

approximation,[51] the EDL thickness at a charged surface is dependent on the solution ionic strength, namely the salt concentration. Theoretically, it varies roughly from 8.7 nm to 0.3 nm if 1 M KCl is added into 1 mM PB solution. **Figure 5b-d** compare the permeation results of three respective molecules upon changing the salt concentration of both feed and permeate solutions (Time-laps movies for permeation of three fluorophores at the high salt concentration can be found in Supplementary **Videos S7–9**). Consistent with the theoretical prediction, as shown in **Figure 5b**, FL^{2-} can permeate through the SNM upon increasing the salt concentration, because of electrostatic screening of both channel surface and dye charges. As for neutral RB, its transmembrane permeation is barely influenced (**Figure 5c**). However, a slower permeation rate was observed for $Ru(bpy)_3^{2+}$ at a higher salt concentration (**Figure 5d**), most likely due to the suppression of the electrostatic attraction force. In addition, the lag time for $Ru(bpy)_3^{2+}$ permeation observed at the low salt concentration, namely ca. 30 s, disappeared at the higher salt concentration. This lag time is much larger than the one calculated from $L_{SNM}^2/6D_h$ (represents the lag time for molecule transport through SNM, where L_{SNM} is the membrane thickness and D_h the hindered diffusion coefficient in the membrane)[52] and $d^2/\pi D_0$ (represents the lag time for molecular transport from SNM edge to detection point, where d is the distance from membrane edge to detection point and D_0 the diffusion coefficient in the bulk solution),[53] namely 46 μs and 1.54 s, respectively. The permeation lag can be also ascribed to the electrostatic interaction. At a low salt concentration, $Ru(bpy)_3^{2+}$ must accumulate in the silica nanochannels or nearby the membrane surface to fully compensate the SNM surface charges before its permeation. In contrast, at a high salt concentration, the electrolyte ions themselves can fully compensate the

silica surface charges, thus $Ru(bpy)_3^{2+}$ can permeate through the SNM directly without delay. Charge-based molecular separation experiments were also conducted with smaller molecules, *e.g.* $Fe(CN)_6^{3-}$ and $Ru(NH_3)_6^{2+}$ (see structures in **Figure S8d**), at both low and high salt concentrations using the electrochemical detection, and similar results were obtained (**Figure S9**). All these data demonstrate that the SNM can separate similarly sized molecules on the basis of their charge, and that the effective channel size of SNM can be also modulated by the salt concentration to control the molecular permeation and its rate.

In addition to the solution ionic strength, the pH can also gate the molecular transport across the SNM. $Ru(bpy)_3^{2+}$ is a perfect fluorophore because its charge and fluorescence intensity do not vary with the solution pH. Its permeation was studied with the solution pH varied from 2 to 6.5 (**Figure S10**). At a high ionic strength, the permeation rate of $Ru(bpy)_3^{2+}$ nearly did not change with the solution pH. Because the membrane surface charge density was fully screened by the high concentration of electrolyte ions, although it varied with the solution pH. In contrast, at a low ionic strength, increasing the solution pH from 3 to 5 led to a remarkably increased permeation rate, due to the change of membrane surface charge from positive to negative. This result also suggests that the SNM surface has an isoelectric point of about 4, which is close to that reported previously for MCM-41 particles.[54, 55]

Molecular Separation after Surface Modification. Membrane surface modification can change the channel size, surface charge (both sign and density), surface wettability and so on. Mesoporous silica surface can be modified by either co-condensation method (changing surface property while retaining pore size) or post-grafting method (changing surface property and pore size simultaneously).[56] Here, we demonstrated that the SNM could exhibit

different molecular separation performance after post-grafting with *N*-trimethoxy-silylpropyl-*N*,*N*,*N*-trimethylammonium chloride (TMAC) monolayer.[10, 57, 58] The surface of modified membrane, abbreviated as SNM-TMAC, became positively charged and meanwhile the channel size was decreased to about 1.7 nm[10, 57, 58]. **Figure 6a** compares the permeation kinetics of FL^{2-} and $Ru(bpy)_3^{2+}$ across the SNM-TMAC. Apparently, only FL^{2-} in the high ionic strength solution can permeate through the membranes. Moreover, the permeation rate is about 10 times lower than that at the pristine SNM (**Figure 5b**), due to the decrease of channel size. The shrunken channels and positively charged surface also drastically hinder the permeation of similarly charged $Ru(bpy)_3^{2+}$, even at the high ionic strength.

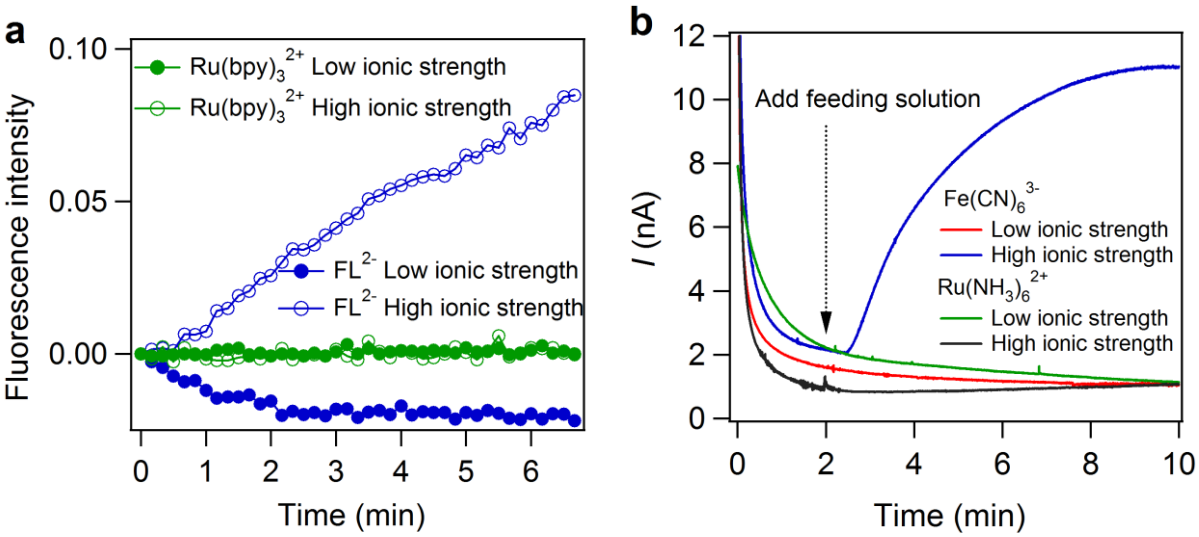

Figure 6. (a) Permeation kinetic plots of FL^{2-} and $Ru(bpy)_3^{2+}$ through SNM-TMAC at the low and high ionic strength. The decreased fluorescence intensity of FL^{2-} at the low ionic strength can be ascribed to the photo bleaching effect. (b) Permeation kinetic plots of $Fe(CN)_6^{3-}$ and $Ru(NH_3)_6^{2+}$ through SNM-TMAC at the low and high ionic strength. The potential applied to working electrode was –0.3 V for the detection of $Fe(CN)_6^{3-}$ and +0.3 V for the detection of $Ru(NH_3)_6^{2+}$.

To eliminate the impact of molecular size, permeation experiments were also conducted with smaller ions, $Fe(CN)_6^{3-}$ and $Ru(NH_3)_6^{2+}$, using the electrochemical detection. The permeation of these two redox probes was akin to that of FL^{2-} and $Ru(bpy)_3^{2+}$, but a relatively small transport rate was found for $Ru(NH_3)_6^{2+}$ at the high ionic strength. As shown in **Figure 6b**, the SNM-TMAC was much more permeable to $Fe(CN)_6^{3-}$ than $Ru(NH_3)_6^{2+}$. On the other hand, the permeation of both FL^{2-} and $Fe(CN)_6^{3-}$ through the positively charged SNM-TMAC was apparently suppressed at the low ionic strength. This phenomenon is in fact contrary to that observed with the pristine SNM, where the oppositely charged ions, for examples $Ru(bpy)_3^{2+}$ (**Figure 5d**) and $Ru(NH_3)_6^{2+}$ (**Figure S9b**), can permeate at a much higher rate at the low ionic strength. This most likely arises from the inhomogeneous surface modification by TMAC, leaving both positively charged groups (quaternary ammonium) and negatively charged ones ($Si\text{-}O^-$) on the nanochannel surface.[10] This zwitterion type surface can act as an ionic barrier that not only repels positively charged molecules but also those negatively charged, in particular at the low ionic strength.[59]

To be noted that the SNM-TMAC can be simply converted back to the pristine SNM by calcination at 550 °C for 6 h. The calcination treatment was often used to burn surfactant templates (*e.g.*, CTAB) in mesoporous silica particles/films. Here, we found that the calcination treatment can also burn out the organic constituents and the fouling pollutants on the SNM, as confirmed by the FL^{2-} permeation test (**Figure S11**). Surface modification with TMAC and calcination removal can be repeated for many times and did not influence the permeation of FL^{2-} significantly.

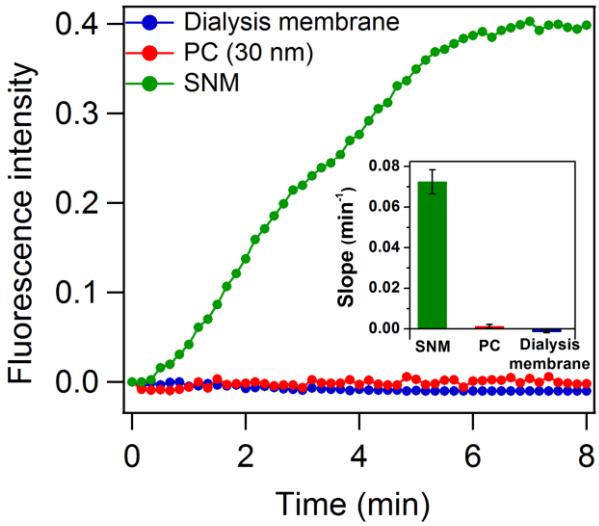

Figure 7. Permeation kinetic plots of FL^{2-} through SNM, spectrum dialysis membrane (molecular cut-off 6 – 8 kD) and track-etched PC membrane (containing 30 nm channels) at a high ionic strength. The inset compares the slopes of these three permeation kinetic plots (Each point was the average of at least three measurements). Note the area for molecular permeation of SNM is about one hundred times smaller than that of commercial membranes.

High Permeation Flux and Membrane Stability. Not only excellent selectivity between molecules with different sizes and/or charges, the SNM also exhibited an extraordinary molecular flux, given its ultrasmall thickness, vertical and parallel channels and very high porosity. Using FL^{2-} as a target of interest (1 mM PB + 1 M KCl), its permeation through the SNM was compared with that through two commercial membranes, namely standard regenerated cellulose dialysis membrane (Spectra/Por 1, molecular cut-off 6 – 8 kD) and track-etched polycarbonate (PC) membrane (containing 30 nm channels). These commercial membranes were put on the top of silicon chip directly for permeation measurements (**Figure S12**). As shown in **Figure 7**, although the effective permeation area of SNM is about one hundred times smaller, the molecular flux through the SNM is several

orders of magnitude larger than dialysis membrane with similar pore size, and even 55 times larger than PC membrane consisting of 30 nm channels.

On the other hand, the SNM displays excellent chemical, thermal and mechanical stability and can be repeatedly used after cleaning by rinse or calcination, though it is ultrathin. Even after being consecutively used for one month, the SNM still covered all the micrometer pores on the p-SiN chip without any obvious cracks and the permeation results were also reproducible (the SEM image, the permeation results, and the operations that SNM experienced in this one month are shown and described in Supplementary **Figure S13**).

Theoretical Consideration. Since the feed and permeate solutions in the microfluidic device were unstirred, the relationship between recorded fluorescence intensity and the number of permeated molecules was hard to quantify precisely. Therefore, we are unable to precisely quantify how many molecules permeate through the SNM at a given time. Nevertheless, in comparison with the molecular separation performance of other membranes[2, 17, 29] that have previously investigated using the similar device, the SNM exhibited a high selectivity towards molecules based on charge or size, due to the ultrasmall channels and very narrow channel size distribution. In addition, although the permeation area of the SNM (2304 μm^2) is much smaller than others (250,000 μm^2 in ref 2 and 90,000 μm^2 in ref. 29), similar molecular flux was obtained. This can be attributed to the high porosity of SNM.

To get a quantitative evaluation, the flux of SNM was compared with that of commercial membranes by examining the flux ratio of FL^{2-} through SNM and PC membrane containing 30 nm channels (J_{SNM}/J_{PC}). The flux, J, can be theoretically calculated by eq 1,

$$J = D_h \times \Delta C \times A_{eff} / L \quad (1)$$

where D_h is the hindered diffusion coefficient of molecules passing through the nanochannel membrane, ΔC the concentration gradient across the membrane, L the membrane thickness and A_{eff} the effective permeation area. D_h can be estimated according to the Renkin equation,[50]

$$D_h = D_0(1-\lambda)^2(1-2.104\lambda+2.09\lambda^3-0.95\lambda^5) \quad (2)$$

where D_0 is the diffusion coefficient of molecule in the bulk solutions. λ is the reduced pore diameter and defined as,

$$\lambda = \frac{\text{Molecule Diameter}}{\text{Pore Diameter}} \quad (3)$$

A_{eff} can be calculated in terms of eq 4,

$$A_{eff} = A_m \times \varepsilon \quad (4)$$

where A_m is the membrane area and ε the porosity.

Hence, by introducing eqs 2 and 4 to eq 1, the flux ratio, J_{SNM}/J_{PC}, can be estimated by the following equation,

$$\frac{J_{SNM}}{J_{PC}} = \frac{D_{h,SNM} \times A_{SNM} \times \varepsilon_{SNM}}{D_{h,PC} \times A_{PC} \times \varepsilon_{PC}} \times \frac{L_{PC}}{L_{SNM}} \quad (5)$$

where $D_{h,SNM}$ and $D_{h,PC}$ denote the hindered diffusion coefficient of molecules passing through the SNM and PC membrane and were calculated to be $0.054D_0$ and $0.86D_0$ (or $0.057D_0$ and $0.81D_0$ calculated from Deen's model[60]), respectively, in terms of eq 2. A_{SNM}/A_{PC} was estimated to be 0.014, considering that A_{SNM} was determined by the micrometer pores on the SiN window. ε_{SNM} and ε_{PC} were 16.7% and 1.3% according to TEM and SEM images of the membranes (**Figure S14**), respectively. L_{PC} and L_{SNM} are 10 μm and 60 nm. Therefore, J_{SNM}/J_{PC} was theoretically calculated to be 1.9.

From the experimental point of view, J_{SNM}/J_{PC} could be roughly regarded as the slope ratio of permeation curve of SNM and PC membrane.[2, 61] Thus, a value of 55 was obtained from **Figure 7**, which is obviously more than one order of magnitude larger than the theoretically calculated value (namely 1.9). This means that either the actual molecular flux across the SNM is much higher or that across the PC membrane is much lower than expected. Given the SNM consists of perpendicular channels of 2.3 nm, is ultrathin and highly porous, we believe that the actual molecular flux across the SNM cannot be predicted by the hindered theory. Indeed, molecule/ion transport in such small nanochannels (usually sub 3-nm) has yet to be rationalized[6, 62]. Many uncertain factors may play important roles, such as the physical structure and hydrodynamic dimension of molecules in the ultrasmall nanochannels, the behavior of water molecules, and their interactions with silanol groups on channel surface (*e.g.*, likely *via* the hydrogen bonding). [6, 62] On the other hand, a lower molecular flux across the PC membrane than that theoretically predicted might result from its hydrophobic surface nature and the possible non-straight channel structure (*e.g.*, asymmetric channel with a small neck in the middle). However, both surface plasma treatment and surface pre-wetting with ethanol/water did not improve the molecular flux, indicating it is not determined by the surface property but most probably the channel size.

CONCLUSIONS

In summary, we report a facile approach for the preparation of ultrathin membrane consisting of perforated silica nanochannels. Due to its ultrasmall thickness (10 – 120 nm), perpendicular channels, uniform channel size (approximately 2.3 nm) and high porosity

(16.7%), the membrane is an excellent filter for molecular separation. Not only a precise selectivity towards molecules based on size and charge but also a high molecular flux was achieved. The membrane displayed excellent chemical, thermal and mechanical stability and could be consecutively used after proper washing or calcination. More importantly, the membrane is advantageous in terms of cost and extremely convenient fabrication process. In addition, the silica surface offers diverse possibilities of chemical modifications to achieve different functionalities. In future, this approach can be utilized to prepare SNMs with different channel size (by changing reaction medium[47] or surfactants[48, 49]), surface property (by one-pot synthesis or post grafting[56]) or channel geometry (*e.g.*, chiral[63]). We believe these membranes will have potential applications in diverse fields: (1) as nanofiltration, ultrafiltration, dialysis and fuel cell separator; (2) for medical diagnostics, drug screening, chemical synthesis and biochemical separation in small sample volumes/analyte quantities by integrating with "lab-on-a-chip" microfluidic systems;[14] (3) for the construction of nanofluidics to study the transport of molecule/ion in nanochannels;[64] (4) for mimicking biological membrane studies due to their similar thickness and ion channel size.

EXPERIMENTAL SECTION

Preparation of SNM/ITO. The SNM was prepared on ITO glass by the Stöber-solution growth approach.[46] Briefly, the ITO glass was firstly cleaned under ultrasonication in 1 M NaOH ethanol solution, acetone, ethanol and water for 15 min sequentially. Subsequently, the ITO glass was immersed in the mixture containing 70 mL water, 30 mL ethanol, 10 μL ammonia aqueous solution, 0.16 g cetyltrimethylammonium bromide (CTAB) and 80 μL

tetraethoxysilane (TEOS). Then, the SNM was grown under quiescent condition at 60 °C. After 4 ~ 24 h, the ITO glass with SNM on it (designated as SNM/ITO) was rinsed with water and then aged at 100 °C overnight. CTAB surfactants existed in the form of micelles in the silica nanochannels were removed by immersing the SNM/ITO in 0.1 M HCl ethanol solution under moderate stirring for 10 min.

Preparation of Perforated SNM. A drop of PMMA solution (3.5 wt %, M_w = 996000) was spin-coated on the SNM/ITO at 2000 rpm for 30 s, followed by solvent evaporation at room temperature for 1 h and then baking at 115 °C for 15 min. Then, the PMMA/SNM/ITO was immersed in 2 M HCl solution overnight to etch the ITO layer, leading to the exfoliation of PMMA/SNM from glass substrate. Subsequently, the free-standing PMMA/SNM was transferred to deionized water, washed and cut into small pieces. Then, a porous substrate was used to fish the PMMA/SNM out of the water and dried at room temperature for 60 min, followed by heating at 100 °C for another 2 h. Finally, the top PMMA layer was removed by immersing in acetone for 6 h.

The porous substrates employed to support the SNM included p-SiN chip (10 mm × 10 mm frame dimension, 1 mm × 1 mm window size, 4 μm pore array and 30 μm pore-to-pore distance), track-etched PET film (2 μm channel size), perforated silicon wafer (25 μm pore size) and capillary plate (10 μm channel size).

Membrane Surface Modification. Membrane modification was performed as reported previously.[57] Briefly, the SNM/p-SiN chip was firstly dried at 100 °C for at least 2 h and then treated with 1% (v/v) *N*-trimethoxy-silylpropyl-*N*,*N*,*N*-trimethylammonium chloride (TMAC) in dry dichloromethane for 4 h at room temperature under stirring. Then, the chip was washed

by dichloromethane and ethanol sequentially under stirring for several times, followed by heating at 80 °C for 2 h.

Evaluation of Membrane Performance. SNM grown for 12 h (60 ± 3 nm) was used in all the permeation experiments unless otherwise mentioned. The measurements were conducted on a device similar to that described in ref. 2 with some modifications. As shown in **Figure 3**, the SNM/p-SiN chip was put on the top of a glass slide with two PDMS gaskets (380 μm thickness) in between, forming a microchannel beneath the SNM. This microchannel was filled with 18 μL blank buffer solution (designated as permeate solution). Then another PDMS film with a 3 mm circular hole was put on the top of SNM to hold the feed solution (5 μL) containing a fluorescent or electrochemical probe. In the fluorescence detection, an inverted fluorescence microscope was used to capture the images every 10 s (Mingmei, Guangzhou, China). The fluorescence intensity at the point of 50 μm far away from the SiN window edge was recorded and plotted against time. In order to compare permeation rate of different molecules, all the measured fluorescence intensity was normalized to that of the equilibrium concentration, namely the concentration after equilibrating 5 μL feed solution with 18 μL permeate solution. In the electrochemical detection, gold working, gold pseudo-reference and platinum counter electrodes were fabricated on the glass chip as described previously,[65] involving standard gold vapor deposition, photolithography and wet chemical etching and platinum electroplating. The width of working, reference and counter electrodes was 50 μm, 50 μm and 200 μm, respectively. The distance between working and reference electrodes was 100 μm, while that between working and counter electrodes was 500 μm.

The concentration of all the fluorescence probes used in the permeation studies was 100 μM unless otherwise mentioned, and that of electrochemical probes was 1 mM. The solutions at a low and higher ionic strength refer to 1 mM PB solution (pH = 6.5) and 1 mM PB + 1 M KCl solution (pH = 6.5). After each permeation experiment, the SNM/p-SiN chip was washed and cleaned by immersing in aqueous solutions for 10 – 60 min. For example, after permeation experiments with FL^{2-}, the chip was cleaned by immersing only in deionized water for 10 min. While for permeation experiments with $Ru(bpy)_3^{2+}$, the membrane was cleaned by immersing in 1 M KCl or 10 mM HCl for 60 min to get rid of surface adsorbed $Ru(bpy)_3^{2+}$. If being highly fouled, the SNM could be also cleaned by calcination at 550 °C for 6 h. All the permeation experiments were performed with individual molecules but not mixture of them. And all the permeation curves from one image were obtained from the same membrane.

To estimate the size of probe molecules, their 3D structures were firstly predicted by COSMOS (http://cosmos.igb.uci.edu/). Then, CHEM 3D was used to measure the distance between molecular center and the farthest atom, which was approximately assumed as the radius of the molecule.

Characterization. SEM images were obtained on a SU8010 field-emission scanning electron microscope. TEM images were obtained on a HT7700 transmission electron microscope at 120 kV. TEM images of transferred SNM were measured by positioning directly 3 mm-in-diameter SNM/p-SiN onto the TEM holder (To be noted that 3 mm-in-diameter p-SiN is commercially fabricated for TEM measurements). Other TEM

specimens were prepared by mechanically scraping small pieces of SNM from ITO glass, dispersion in ethanol and then deposition on carbon-coated copper grids.

Conflict of Interest: The authors declare no competing financial interest.

AUTHOR INFORMATION

Corresponding Author

* Correspondence and request for materials should be addressed to B.S. (e-mail: subin@zju.edu.cn)

Author Contributions

The manuscript was written through contributions of all authors. All authors have given approval to the final version of the manuscript.

Supporting information

The materials used, more SEM and TEM images, and more permeation results can be found in supporting information. This material is available free of charge *via* the Internet at http://pubs.acs.org.

Acknowledgment

This work was supported by the Nature Science Foundation of China (21222504, 21335001), the Zhejiang Provincial Natural Science Foundation (LR14B050001) and the Fundamental Research Funds for the Central Universities (2014XZZX003-04, 2014FZA3006).

REFERENCES

1. Yamaguchi, A.; Uejo, F.; Yoda, T.; Uchida, T.; Tanamura, Y.; Yamashita, T.; Teramae, N. Self-Assembly of a Silica–Surfactant Nanocomposite in a Porous Alumina Membrane. *Nat. Mater.* **2004**, *3*, 337-341.
2. Striemer, C. C.; Gaborski, T. R.; McGrath, J. L.; Fauchet, P. M. Charge-and Size-Based Separation of Macromolecules Using Ultrathin Silicon Membranes. *Nature* **2007**, *445*, 749-753.
3. Gaborski, T. R.; Snyder, J. L.; Striemer, C. C.; Fang, D. Z.; Hoffman, M.; Fauchet, P. M.; McGrath, J. L. High-Performance Separation of Nanoparticles with Ultrathin Porous Nanocrystalline Silicon Membranes. *ACS Nano* **2010**, *4*, 6973-6981.
4. Surwade, S. P.; Smirnov, S. N.; Vlassiouk, I. V.; Unocic, R. R.; Veith, G. M.; Dai, S.; Mahurin, S. M. Water Desalination Using Nanoporous Single-Layer Graphene. *Nat. Nanotechnol.* **2015**, *10*, 459-464.
5. de la Escosura-Muñiz, A.; Merkoçi, A. Nanochannels Preparation and Application in Biosensing. *ACS Nano* **2012**, *6*, 7556-7583.
6. Duan, C.; Majumdar, A. Anomalous Ion Transport in 2-Nm Hydrophilic Nanochannels. *Nat. Nanotechnol.* **2010**, *5*, 848-852.
7. Howorka, S.; Siwy, Z. Nanopore Analytics: Sensing of Single Molecules. *Chem. Soc. Rev.* **2009**, *38*, 2360-2384.
8. Zheng, Z.; Huang, X.; Schenderlein, M.; Möhwald, H.; Xu, G. K.; Shchukin, D. G. Bioinspired Nanovalves with Selective Permeability and pH Sensitivity. *Nanoscale* **2015**, *7*, 2409-2416.
9. Jeon, G.; Yang, S. Y.; Kim, J. K. Functional Nanoporous Membranes for Drug Delivery. *J. Mater. Chem.* **2012**, *22*, 14814-14834.
10. Yamaguchi, A.; Namekawa, M.; Kamijo, T.; Itoh, T.; Teramae, N. Acid−Base Equilibria inside Amine-Functionalized Mesoporous Silica. *Anal. Chem.* **2011**, *83*, 2939-2946.
11. Algara-Siller, G.; Lehtinen, O.; Wang, F. C.; Nair, R. R.; Kaiser, U.; Wu, H. A.; Geim, A. K.; Grigorieva, I. V. Square Ice in Graphene Nanocapillaries. *Nature* **2015**, *519*, 443-445.
12. Kim, E.; Xiong, H.; Striemer, C. C.; Fang, D. Z.; Fauchet, P. M.; McGrath, J. L.; Amemiya, S. A Structure-Permeability Relationship of Ultrathin Nanoporous Silicon Membrane: A Comparison with the Nuclear Envelope. *J. Am. Chem. Soc.* **2008**, *130*, 4230-4231.
13. Fornasiero, F.; Park, H. G.; Holt, J. K.; Stadermann, M.; Grigoropoulos, C. P.; Noy, A.; Bakajin, O. Ion Exclusion by Sub-2-Nm Carbon Nanotube Pores. *Proc. Natl. Acad. Sci. U. S. A.* **2008**, *105*, 17250-17255.
14. van den Berg, A.; Wessling, M. Nanofluidics: Silicon for the Perfect Membrane. *Nature* **2007**, *445*, 726-726.
15. Deng, C.; Zhang, Q. G.; Han, G. L.; Gong, Y.; Zhu, A. M.; Liu, Q. L. Ultrathin Self-Assembled Anionic Polymer Membranes for Superfast Size-Selective Separation. *Nanoscale* **2013**, *5*, 11028-11034.
16. Martin, C. R.; Siwy, Z. Molecular Filters - Pores within Pores. *Nat. Mater.* **2004**, *3*, 284-285.
17. Choi, D.-H.; Han, Y. D.; Lee, B.-K.; Choi, S.-J.; Yoon, H. C.; Lee, D.-S.; Yoon, J.-B. Use of a Columnar Metal Thin Film as a Nanosieve with Sub-10 Nm Pores. *Adv. Mater.* **2012**, *24*, 4408-4413.
18. Feng, D.; Lv, Y.; Wu, Z.; Dou, Y.; Han, L.; Sun, Z.; Xia, Y.; Zheng, G.; Zhao, D. Free-Standing Mesoporous Carbon Thin Films with Highly Ordered Pore Architectures for Nanodevices. *J. Am. Chem. Soc.* **2011**, *133*, 15148-15156.
19. Joshi, R. K.; Carbone, P.; Wang, F. C.; Kravets, V. G.; Su, Y.; Grigorieva, I. V.; Wu, H. A.; Geim, A. K.; Nair, R. R. Precise and Ultrafast Molecular Sieving through Graphene Oxide Membranes. *Science* **2014**, *343*, 752-754.
20. O'Hern, S. C.; Boutilier, M. S.; Idrobo, J. C.; Song, Y.; Kong, J.; Laoui, T.; Atieh, M.; Karnik, R. Selective

Ionic Transport through Tunable Subnanometer Pores in Single-Layer Graphene Membranes. *Nano Lett.* **2014**, *14*, 1234-1241.

21. Hinds, B. J.; Chopra, N.; Rantell, T.; Andrews, R.; Gavalas, V.; Bachas, L. G. Aligned Multiwalled Carbon Nanotube Membranes. *Science* **2004**, *303*, 62-65.
22. Holt, J. K.; Park, H. G.; Wang, Y.; Stadermann, M.; Artyukhin, A. B.; Grigoropoulos, C. P.; Noy, A.; Bakajin, O. Fast Mass Transport through Sub-2-Nanometer Carbon Nanotubes. *Science* **2006**, *312*, 1034-1037.
23. Kohli, P.; Harrell, C. C.; Cao, Z.; Gasparac, R.; Tan, W.; Martin, C. R. DNA-Functionalized Nanotube Membranes with Single-Base Mismatch Selectivity. *Science* **2004**, *305*, 984-986.
24. Savariar, E. N.; Krishnamoorthy, K.; Thayumanavan, S. Molecular Discrimination inside Polymer Nanotubules. *Nat. Nanotechnol.* **2008**, *3*, 112-117.
25. Warkiani, M. E.; Bhagat, A. A. S.; Khoo, B. L.; Han, J.; Lim, C. T.; Gong, H. Q.; Fane, A. G. Isoporous Micro/Nanoengineered Membranes. *ACS Nano* **2013**, *7*, 1882-1904.
26. Tong, H. D.; Jansen, H. V.; Gadgil, V. J.; Bostan, C. G.; Berenschot, E.; van Rijn, C. J. M.; Elwenspoek, M. Silicon Nitride Nanosieve Membrane. *Nano Lett.* **2004**, *4*, 283-287.
27. El-Safty, S.; Shahat, A.; Awual, M. R.; Mekawy, M. Large Three-Dimensional Mesocage Pores Tailoring Silica Nanotubes as Membrane Filters: Nanofiltration and Permeation Flux of Proteins. *J. Mater. Chem.* **2011**, *21*, 5593-5603.
28. Lee, S. B.; Mitchell, D. T.; Trofin, L.; Nevanen, T. K.; Soderlund, H.; Martin, C. R. Antibody-Based Bio-Nanotube Membranes for Enantiomeric Drug Separations. *Science* **2002**, *296*, 2198-2200.
29. Vlassiouk, I.; Apel, P. Y.; Dmitriev, S. N.; Healy, K.; Siwy, Z. S. Versatile Ultrathin Nanoporous Silicon Nitride Membranes. *Proc. Natl. Acad. Sci. U. S. A.* **2009**, *106*, 21039-21044.
30. Jirage, K. B. Nanotubule-Based Molecular-Filtration Membranes. *Science* **1997**, *278*, 655-658.
31. Asatekin, A.; Gleason, K. K. Polymeric Nanopore Membranes for Hydrophobicity-Based Separations by Conformal Initiated Chemical Vapor Deposition. *Nano Lett.* **2011**, *11*, 677-686.
32. Yang, S. Y.; Ryu, I.; Kim, H. Y.; Kim, J. K.; Jang, S. K.; Russell, T. P. Nanoporous Membranes with Ultrahigh Selectivity and Flux for the Filtration of Viruses. *Adv. Mater.* **2006**, *18*, 709-712.
33. Qiu, X.; Yu, H.; Karunakaran, M.; Pradeep, N.; Nunes, S. P.; Peinemann, K.-V. Selective Separation of Similarly Sized Proteins with Tunable Nanoporous Block Copolymer Membranes. *ACS Nano* **2012**, *7*, 768-776.
34. Uehara, H.; Kakiage, M.; Sekiya, M.; Sakuma, D.; Yamonobe, T.; Takano, N.; Barraud, A.; Meurville, E.; Ryser, P. Size-Selective Diffusion in Nanoporous but Flexible Membranes for Glucose Sensors. *ACS Nano* **2009**, *3*, 924-932.
35. Geng, J.; Kim, K.; Zhang, J.; Escalada, A.; Tunuguntla, R.; Comolli, L. R.; Allen, F. I.; Shnyrova, A. V.; Cho, K. R.; Munoz, D.; Wang, Y. M.; Grigoropoulos, C. P.; Ajo-Franklin, C. M.; Frolov, V. A.; Noy, A. Stochastic Transport through Carbon Nanotubes in Lipid Bilayers and Live Cell Membranes. *Nature* **2014**, *514*, 612-615.
36. López-Lorente, A.; Simonet, B.; Valcárcel, M. The Potential of Carbon Nanotube Membranes for Analytical Separations. *Anal. Chem.* **2010**, *82*, 5399-5407.
37. Huang, H.; Song, Z.; Wei, N.; Shi, L.; Mao, Y.; Ying, Y.; Sun, L.; Xu, Z.; Peng, X. Ultrafast Viscous Water Flow through Nanostrand-Channelled Graphene Oxide Membranes. *Nat. Commun.* **2013**, *4*, 1-9.
38. Wu, J.; Gerstandt, K.; Zhang, H.; Liu, J.; Hinds, B. J. Electrophoretically Induced Aqueous Flow through Single-Walled Carbon Nanotube Membranes. *Nat. Nanotechnol.* **2012**, *7*, 133-139.
39. Majumder, M.; Chopra, N.; Hinds, B. J. Mass Transport through Carbon Nanotube Membranes in Three

Different Regimes: Ionic Diffusion and Gas and Liquid Flow. *ACS Nano* **2011**, *5*, 3867-3877.

40. Majumder, M.; Chopra, N.; Hinds, B. J. Effect of Tip Functionalization on Transport through Vertically Oriented Carbon Nanotube Membranes. *J. Am. Chem. Soc.* **2005**, *127*, 9062-9070.
41. Wu, J.; Gerstandt, K.; Majumder, M.; Zhan, X.; Hinds, B. J. Highly Efficient Electroosmotic Flow through Functionalized Carbon Nanotube Membranes. *Nanoscale* **2011**, *3*, 3321-8.
42. Yeh, C.-N.; Raidongia, K.; Shao, J.; Yang, Q.-H.; Huang, J. On the Origin of the Stability of Graphene Oxide Membranes in Water. *Nat. Chem.* **2015**, *7*, 166-170.
43. Celebi, K.; Buchheim, J.; Wyss, R. M.; Droudian, A.; Gasser, P.; Shorubalko, I.; Kye, J.-I.; Lee, C.; Park, H. G. Ultimate Permeation across Atomically Thin Porous Graphene. *Science* **2014**, *344*, 289-292.
44. Urbanova, V.; Walcarius, A. Vertically-Aligned Mesoporous Silica Films. *Z. Anorg. Allg. Chem.* **2014**, *640*, 537-546.
45. Walcarius, A.; Sibottier, E.; Etienne, M.; Ghanbaja, J. Electrochemically Assisted Self-Assembly of Mesoporous Silica Thin Films. *Nat. Mater.* **2007**, *6*, 602-608.
46. Teng, Z.; Zheng, G.; Dou, Y.; Li, W.; Mou, C.-Y.; Zhang, X.; Asiri, A. M.; Zhao, D. Highly Ordered Mesoporous Silica Films with Perpendicular Mesochannels by a Simple Stober-Solution Growth Approach. *Angew. Chem. Int. Ed.* **2012**, *51*, 2173-2177.
47. Kao, K. C.; Lin, C. H.; Chen, T. Y.; Liu, Y. H.; Mou, C. Y. A General Method for Growing Large Area Mesoporous Silica Thin Films on Flat Substrates with Perpendicular Nanochannels. *J. Am. Chem. Soc.* **2015**, *137*, 3779-3782.
48. Goux, A.; Etienne, M.; Aubert, E.; Lecomte, C.; Ghanbaja, J.; Walcarius, A. Oriented Mesoporous Silica Films Obtained by Electro-Assisted Self-Assembly. *Chem. Mater.* **2009**, *21*, 731-741.
49. Robertson, C.; Beanland, R.; Boden, S. A.; Hector, A. L.; Kashtiban, R. J.; Sloan, J.; Smith, D. C.; Walcarius, A. Ordered Mesoporous Silica Films with Pores Oriented Perpendicular to a Titanium Nitride Substrate. *Phys. Chem. Chem. Phys.* **2015**, *17*, 4763-4770.
50. Renkin, E. M. Filtration, Diffusion, and Molecular Sieving through Porous Cellulose Membranes. *J. Gen. Physiol.* **1954**, *38*, 225-243.
51. Schoch, R. B.; Han, J.; Renaud, P. Transport Phenomena in Nanofluidics. *Rev. Mod. Phys.* **2008**, *80*, 839-883.
52. Kontturi, K.; Murtomäki, L.; Manzanares, J. A. *Ionic Transport Processes: In Electrochemistry and Membrane Science*. Oxford University Press, Oxford: 2008.
53. Bard, A. J.; Faulkner, L. R. *Electrochemical Methods: Fundamentals and Applications*. 2nd ed.; Wiley, New York: 2001; Vol. 2.
54. Musso, G.; Bottinelli, E.; Celi, L.; Magnacca, G.; Berlier, G. Influence of Surface Functionalization on the Hydrophilic Character of Mesoporous Silica Nanoparticles. *Phys. Chem. Chem. Phys.* **2015**, *17*, 13882-13894.
55. Liu, W.; Liu, J.; Yang, X.; Wang, K.; Wang, Q.; Yang, M.; Li, L.; Xu, J. Ph and Ion Strength Modulated Ionic Species Loading in Mesoporous Silica Nanoparticles. *Nanotechnology* **2013**, *24*, 415501.
56. Hoffmann, F.; Cornelius, M.; Morell, J.; Froba, M. Silica-Based Mesoporous Organic-Inorganic Hybrid Materials. *Angew. Chem. Int. Ed.* **2006**, *45*, 3216-3251.
57. Li, W.; Ding, L.; Wang, Q.; Su, B. Differential Pulse Voltammetry Detection of Dopamine and Ascorbic Acid by Permselective Silica Mesochannels Vertically Attached to the Electrode Surface. *Analyst* **2014**, *139*, 3926-3931.
58. Fattakhovarohlfing, D.; Wark, M.; Rathousky, J. Electrode Layers for Electrochemical Applications Based on Functionalized Mesoporous Silica Films. *Sensors and Actuators B: Chemical* **2007**, *126*, 78-81.

59. Calvo, A.; Yameen, B.; Williams, F. J.; Soler-Illia, G. J.; Azzaroni, O. Mesoporous Films and Polymer Brushes Helping Each Other to Modulate Ionic Transport in Nanoconfined Environments. An Interesting Example of Synergism in Functional Hybrid Assemblies. *J. Am. Chem. Soc.* **2009**, *131*, 10866-10868.
60. Dechadilok, P.; Deen, W. M. Hindrance Factors for Diffusion and Convection in Pores. *Ind. Eng. Chem. Res.* **2006**, *45*, 6953-6959.
61. Snyder, J. L.; Clark, A.; Fang, D. Z.; Gaborski, T. R.; Striemer, C. C.; Fauchet, P. M.; McGrath, J. L. An Experimental and Theoretical Analysis of Molecular Separations by Diffusion through Ultrathin Nanoporous Membranes. *J. Membr. Sci.* **2011**, *369*, 119-129.
62. Daiguji, H. Ion Transport in Nanofluidic Channels. *Chem. Soc. Rev.* **2010**, *39*, 901-911.
63. Shopsowitz, K. E.; Qi, H.; Hamad, W. Y.; Maclachlan, M. J. Free-Standing Mesoporous Silica Films with Tunable Chiral Nematic Structures. *Nature* **2010**, *468*, 422-425.
64. Fan, R.; Huh, S.; Yan, R.; Arnold, J.; Yang, P. Gated Proton Transport in Aligned Mesoporous Silica Films. *Nat. Mater.* **2008**, *7*, 303-307.
65. Lin, X.; Hu, X.; Bai, Z.; He, Q.; Chen, H.; Yan, Y.; Ding, Z. A Microfluidic Chip Capable of Switching W/O Droplets to Vertical Laminar Flow for Electrochemical Detection of Droplet Contents. *Anal. Chim. Acta* **2014**, *828*, 70-79.